J Mater Sci (2023) 58:8981–8989

Metals & corrosion

Pockets of strain-softening and strain-hardening in high-strength Cu-24wt%Ag sheets

Rongmei Niu[1] and Ke Han[1,*]

[1] *National High Magnetic Field Laboratory, Florida State University, 1800 E Paul Dirac Dr. , Tallahassee, FL 32310, USA*

Received: 20 January 2023
Accepted: 20 April 2023

ABSTRACT

To study plastic deformation behavior in high-strength Cu–Ag nanostructured composites, we compared (1) overall stress–strain curves with local stress–strain curves and (2) engineering stress–strain curves with true stress–strain curves. We then related the differences between these curves to the internal structure of the composites from microscale to atomic scale. Strain-softening appeared both locally and overall in longitudinal samples. Pronounced strain-hardening occurred only locally in transversal samples. In longitudinal cross-section, but not in transversal cross-section, we observed many shear bands in which the lamellar thickness values of Cu and Ag were below 6 nm and 2 nm, respectively. Within these bands, the boundaries between Cu and Ag were composed of semi-coherent {111} interfaces in a zigzag pattern, with twins and stacking faults concentrated in Ag lamellae. We demonstrated that strain-softening in longitudinal tensile samples resulted from a favorable angle within shear bands between the existing {111} slip system and the maximum shear stress direction. Strength in the transverse direction was about 10% stronger than in the longitudinal direction, an anisotropy in strength values that we attributed to the underlying anisotropy in local true strain-hardening.

Introduction

Heavily drawn Cu-based composites (Cu–Ag, Cu-Nb, Cu-Cr, and the like) have been studied extensively both experimentally and theoretically [1–11]. In these composites, the Cu matrix is strengthened by either one dimensional fiber or two-dimensional ribbon [12–17]. Such low dimensional nanosized components have other applications as well [18]. The strength of such composites is much higher than that predicted by the rule of mixtures. A previous study, for example, showed that an ultimate tensile strength (UTS) of 1.45 GPa was realized in Cu-24 wt% Ag wire at a draw ratio of 5.8 [19]. An extraordinary enhancement of the work hardening rate was observed.

Handling Editor: Catalin Croitoru.

Address correspondence to E-mail: han@magnet.fsu.edu

https://doi.org/10.1007/s10853-023-08519-y

Cu–Ag nano-composite sheets are especially useful as high-performance conductors in electronic devices because of their optimized combination of mechanical strength and electrical conductivity [5]. In these sheets, we had previously observed strong anisotropy of mechanical properties [20]. This strong anisotropy was qualitatively related to local shear anisotropy and overall texture. In this current study, we evaluated the strain-hardening capacity of these sheets and related this capacity to microstructure in a variety of scales in order to quantitatively study this anisotropic behavior.

Ductility can be measured by three parameters: elongation-to-failure, bending strain, and reduction-in-area. Although the elongation-to-failure of microstructured Cu–Ag is greater than 10%, the elongation-to-failure of nanostructured Cu-24%Ag sheets (with a strength of ~ 900 MPa) is only ~ 3% [20–23]. One reason that high-strength materials have low values for elongation-to-failure may be that they also have low strain-hardening rates. In fact, some researchers have found no indication at all of strain-hardening in either engineering stress–strain curves or true stress–strain curves for nanostructured Cu–Ag sheets [20–22]. Because of its low strain-hardening rate, high-strength Cu–Ag under small deformation strain is prone to localized deformation known as "necking." According to the ASTM standard, which seeks to deemphasize purely local deformation in favor of overall deformation, elongation-to-failure must be measured as an average value in a sample with a relatively long gauge length. We found that most of the deformation in high-strength Cu–Ag occurred within the necking area (usually less than 1 mm in length), which is by definition local. Therefore, the elongation-to-failure values derived using the ASTM standard are inconsistent with other ductility parameters in nanostructured Cu–Ag. In this material, researchers have found large bending strain (up to 59%) and large reduction-in-area (up to 60%) [3, 22]. Our hypothesis is that there is a discrepancy between local deformation and average deformation because of inhomogeneous strain-hardening during deformation. This study addresses strain-hardening behavior in high-strength Cu–Ag within regions of various strain levels.

Experimental methods

Materials

The material used in this work was 0.67 mm-thick Cu-24wt%Ag sheets manufactured by Tanaka. The tensile test specimens were fabricated according to ASTM standard E8M specification, with respect to the rolling direction. Tensile samples were made with a gauge length of 50 mm and a gage width of 8.78 mm in a dog bone shape. Longitudinal direction samples (LD) were made parallel to the rolling direction (RD), and transversal ones (TD) were made perpendicular to the rolling direction.

Tensile tests

Tensile tests, under displacement control at a rate of 0.3 mm/min, were performed at 295 K on a servo-hydraulic MTS test machine. A 25 mm clip-on extensometer was used to record strain, and a 10 kN load cell was used to measure force. A digital image correlation (DIC) system was employed to monitor the in-situ strain field on sheets held under tension. DIC revealed that, shortly before the failure of the samples, strain distribution concentrated mainly in local necking areas (see Fig. 2). We speculated that the formation of necking was closely tied to work hardening, so we recorded the strain values of a certain local spot in the necking (P_0, 0.1mm × 0.1 mm) for strain-hardening analysis.

Microstructure characterizations

Fractography and the distribution of shear bands were examined by dual-beam scanning electron microscopy (Helios_FIB_FEI). Using JEM-ARM200CF STEM, we observed the lamellar structure of Cu–Ag sheets along the longitudinal x-section. The TEM x-section samples were prepared by an electro-polishing method described by previous researchers [24]. In our current study, x-section TEM samples were dimpled to ~ 15 µm, then subjected to argon ion-milling at 3 kV at 7°. High-Angle Annular-Dark-Field STEM (HAADF-STEM) studies were carried out using a probe-aberration-corrected, cold-field-emission JEM JEOL ARM 200cF at 200 kV. We acquired HAADF-STEM images using a 30-µm condenser lens aperture at a camera length of 7 cm, a combination that corresponds to a collection

Table 1 Mechanical properties of 0.67 mm-thick Cu-24 wt%Ag sheets

Tensile axis orientation		LD	TD
Young's Modulus, GPa	Extensometer	109	128
	DIC	100	123
Ultimate tensile strength, MPa	Eng	915 ± 1	992 ± 6
	Tru	930 ± 2	1163 ± 6
Elongation, %	DIC at P_0, 0.1 × 0.1mm^2 in slip bands	30.8 ± 2.1	24.3 ± 3.5
	Extensometer	3.6 ± 0.4	4.8 ± 0.4
Reduction-in-width, %		6.3 ± 0.7	11.0 ± 0.7

angle of 58.7 mrad. The image-scanning speed was 32 µs/pixel. The beam convergent angle was 21 mrad.

Results and discussion

Strain-softening/hardening anisotropy

Our samples showed anisotropy in mechanical properties. This is consistent with previous research results [20]. We found that Young's modulus measured longitudinally in our samples, where the texture was < 111 > , was ~ 15% lower than that measured transversally, where no clearly defined texture could be detected. Young's modulus in textured materials is known to be dependent on the crystal orientation of the grains [25, 26]. Tensile strength in all our Cu–Ag sheets was also anisotropic, i.e., ultimate tensile strength in the longitudinal direction averaged 9% lower than in the transversal direction. Macroscale elongation, as measured by extensometer, displayed only a small difference between the two directions, and macroscale uniform elongation, measured as 0.9%, displayed no difference (as shown in Table 1). Engineering stress-strain curves in Cu-Ag sheets showed no strain-hardening at all under tensile stress (Fig. 1, Table 2).

Our macroscale data provided no explanation for the contradiction that we observed between strong strength anisotropy and weak elongation anisotropy, so we examined local strain distribution in different orientations. The local and overall strain-softening rates were estimated by comparing overall stress–strain curves (measured by extensometer) with local stress–strain curves (measured by DIC at certain locations in the necking region, see P_{0L} and P_{0T} in Fig. 2). The resulting engineering stress–strain curves showed softening in both cases, but the local softening rate was one order of magnitude lower than the overall softening rate, indicating the occurrence of large plastic deformation in the necking region (Table 1). Such high elongation in this region indicates delayed necking, probably as a result of local work hardening. Accordingly, we plotted the true stress–strain curve (see Fig. 1) and measured the stress and strain in a selected necking area (see P_{0L} in Fig. 2). Both the true and engineering stress values decreased with tension strain in longitudinal samples, indicating strain-softening, but the true stress–strain curve in the necking region in transversal samples (such as P_{0T} in Fig. 2) exhibited a different trend, indicating pronounced strain-hardening.

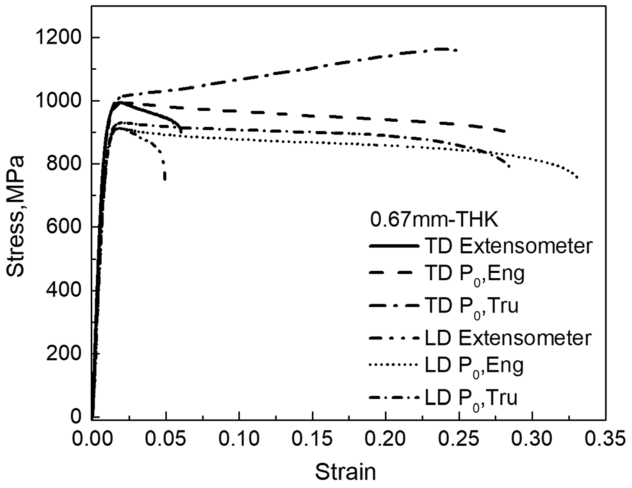

Figure 1 Stress–strain curves of high-strength Cu–Ag sheets. Macro and local stress–strain curves were, respectively, plotted using strain data collected by the extensometer and by DIC at P_0, an area of 0.1 × 0.1mm^2 within the necking bands. True stress–strain curves were indicated by Eng and Tru, respectively.

Local plasticity anisotropy

During tension, we found, the straight edges of samples tapered inward, forming a "necking region," where the magnitude of elongation anisotropy became severe, resulting in a shorter necking region

Table 2 Strain-softening/hardening rate

Strain/Stress	Orientation	Location	Softening/Hardening rates* (MPa)
Engineering	Longitudinal	Local	− 328
	Longitudinal	Overall	− 2259
	Transversal	Local	− 303
	Transversal	Overall	− 1574
True			
	Longitudinal	Local	− 219
	Transversal	Local	698

*Softening/Hardening rates were calculated from the slope of the stress–strain curve after yielding

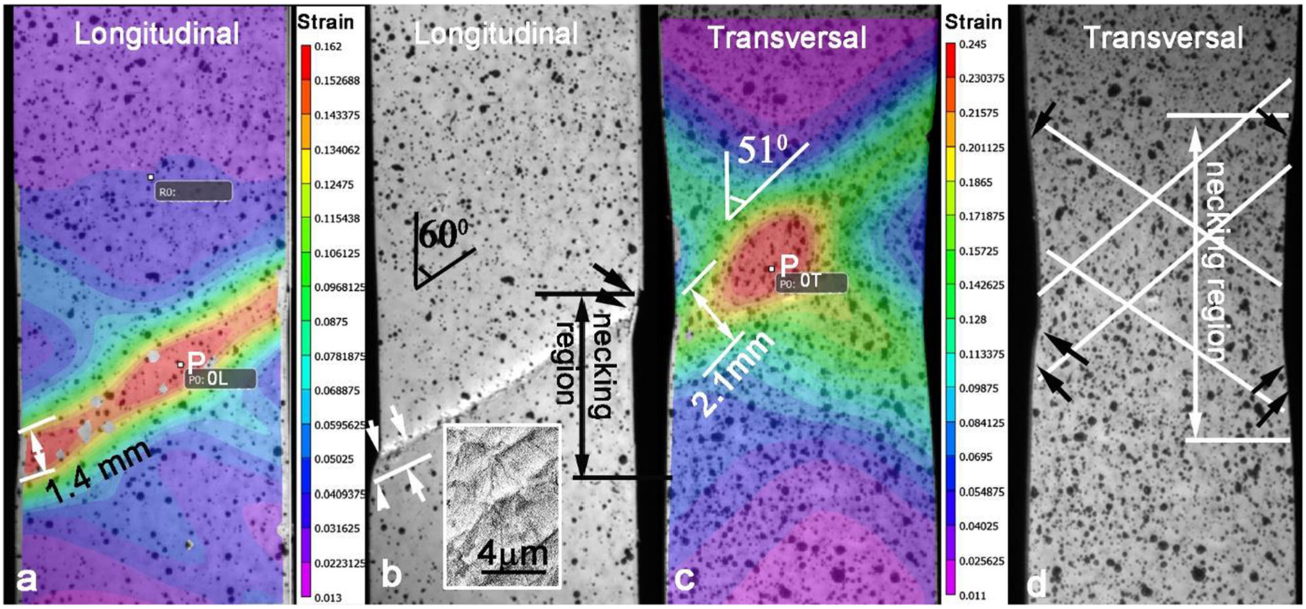

Figure 2 Strain data, collected by DIC, from samples under tension. The colors in Figs a and c represent local tension strain values calculated from the original images. The correlation between strain values and the spectrum of colors is shown in the narrow vertical charts attached to the right of Fig a and c. Figure b and d show typical original images of two samples. a. Strain distribution in a typical longitudinal sample approaching fracture. The highest strain region, represented by a red band with an average width of 1.4 mm, may reflect the presence of a cluster of slip bands. b. Corresponding raw image of Fig. 2a with a pronounced 1.4 mm-wide cluster of slip bands(as indicated in the inset) that inclines ~ 60° to the tensile axis. In the necking area, slight curvatures (leading to a reduction-in-width of 6.3 ± 0.7%) appear at the sample edges. These curvatures appear more pronounced in Fig. b than in Fig. a. c. Typical strain distribution in transversal samples before fracture, with the red band (region of highest strain) about 2.1 mm wide. The angle between this band and the tensile axis is ~ 51°. d. Corresponding image of Fig. 2c showing a large area of necking (reduction-in-width of 11.0 ± 0.7%).

in longitudinal samples (6.4 mm) than in transversal ones (10.5 mm). The presence of slip bands on the surface of the samples indicated that multiple slipping had occurred. These localized necking bands were connected by short arcs, unlike the long arcs often found by other researchers studying single phase samples with larger grains [27]. In our study, the necking bands (from now on indistinctly referred to as necking bands) inclined ~ 60° to the tension axis in LD and ~ 51° to the tension axis in TD (Fig. 2). This anisotropy in the slipping direction led not only to a local elongation anisotropy, but also to a difference in reduction-in-width, from 6.3 ± 0.7% in longitudinal samples to 11.0 ± 0.7% in transversal samples.

The width of the necking bands before failure was 1.4 mm in LD and 2.1 mm in TD (see Fig. 2a, c). Even though the LD had a shorter necking region, its local elongation reached as high as 30.8 ± 3% within the slip band, compared to only 24.3 ± 2% within the

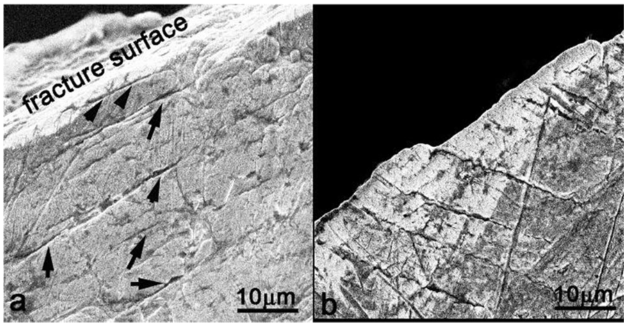

Figure 3 Cracks around the primary fracture by SEM. a. straight cracks, indicated by black arrows, in longitudinal samples. The cracks are parallel to the shear fracture, reflecting the existence of texture in the sheet rolling direction. b. a transversal sample with secondary cracks. These cracks propagate in directions other than that of the primary fracture.

slip bands of the TD (see area P_{0L} in Fig. 2). Local elongation values were much higher than the macroscale elongation values that had been measured by extensometer.

Along the necking bands, the typical failure in our CuAg sheets was a shear fracture. Within the necking bands of longitudinal samples, but not those of transversal samples, many long, straight cracks appeared parallel to the primary fracture (see Fig. 3). The thickness values of most necking regions were measured to be ~ 263 µm in longitudinal samples and ~ 532 µm in transversal ones. The average thickness reductions were ~ 47.6 ± 8% and ~ 13.2 ± 5% in each case, as shown in Online Resource 1.

To analyze the anisotropic plastic behavior in our rolled sheet quantitatively, we calculated the Lankford parameter or anisotropy coefficient using our uniaxial tensile tests on sheet specimens. The anisotropy coefficient (r) is defined by [28]:

$$r = \varepsilon_w^p / \varepsilon_t^p = \ln\left(\frac{w}{w_0}\right) / \ln\left(\frac{t}{t_0}\right) \tag{1}$$

where $\varepsilon^P{}_w$ and $\varepsilon^P{}_t$ are the plastic strains in the width (w) and thickness (t) directions, respectively. w_0 and w are the initial and final widths, while t_o and t are the initial and final thickness, respectively, of the specimen. Taking into account the condition of volume constancy, Eq. 1 can be rearranged as follows:

$$r = \frac{-\ln\left(\frac{w}{w_0}\right)}{ln\left(\frac{l}{l_0}\right) + ln\left(\frac{w}{w_0}\right)} \tag{2}$$

Table 3 Lankford coefficient r and localization angle calculation

	Before necking		After necking, at P_0	
	LD	TD	LD	TD
Elongation, %	2.2	2.5	30.8	24.3
Width reduction, %	0.4	1.6	6.3	11.0
$\ln l/l_0$	0.022	0.025	0.269	0.218
$\ln w/w_0$	0.004	0.016	− 0.065	− 0.117
r	0.15	0.39	0.32	1.15
θ, °C	70.4	62.0	63.8	53.8

where l_0 and l are the initial and final gauge lengths. In most of materials, the most anisotropic behavior ($r \neq 1$) is observed in LD and TD, whereas rather isotropic behave ($r \approx 1$) is observed at 45 to the LD[29]. Using Eq. 2, we calculated the coefficient at P_0 location in our Cu–Ag sheets. Before necking, the coefficient was about 0.15 in LD and 0.39 in TD. After necking, it was around 0.32 in LD and 1.15 TD (see Table 3). The results indicated that, even at the uniform deformation stage, the anisotropic exhibited, and it became stronger after necking.

Based on the correlations of the Lankford coefficient and the necking bands, we estimated the inclination angles of the necking bands, θ (the angle between the band length and the tensile direction [30–32]).

$$\theta = \frac{\pi}{2} - \tan^{-1}\sqrt{\frac{r}{1+r}} \tag{3}$$

Before necking, the inclination angles were around 70.4° in LD and 62.0° in TD to the tensile direction. After that, they stabilized at 63.8° in LD and 53.8° in TD. The angles reduced in both directions with the preceding necking. These angles were different from the necking band angles of 60° in LD and 51° in TD (Fig. 2). This difference, however, was within measurement error of the strain values. For an isotropic material, the necking bands are at 54.76° to the loading axis [31]. LD Cu–Ag samples showed strong anisotropic behavior by demonstrating the orientation of the necking bands with respect to tension axis very far from ~ 55°. TD samples showed isotropic behavior by demonstrating a ~ 55° angle.

Earlier research found < 111 > texture running parallel to the longitudinal direction in Cu–Ag composite sheets that had been deformed to about 97% reduction-in-thickness, even though the orientation remained random in the transversal direction [20].

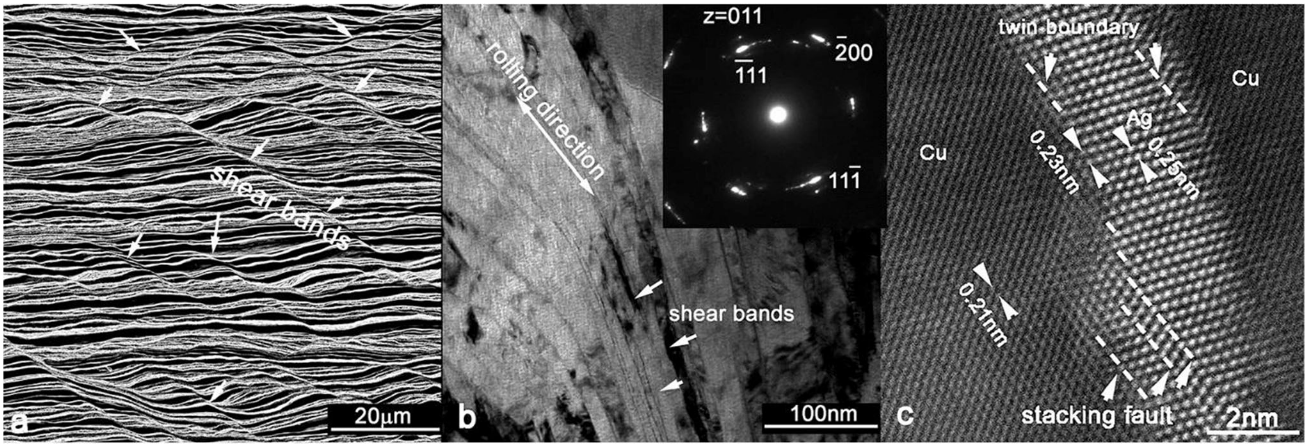

Figure 4 Microscopy images on longitudinal x-section. a. SEM image of shear bands (indicated by white arrows). b. TEM image of the lamellar structure and shear bands (some of which are indicated by white arrows) on the longitudinal x-section. Lamellar spacing is ~ 35 nm. Lamellae in shear band areas are finer than in other areas: the width of Ag lamellae is < 2 nm, and Cu lamellae < 6 nm. The inset shows a selected area diffraction pattern in the shear band. The short, curved diffraction spots in {111} or *{200}* indicate the presence of textured nano lamellae. Of the two opposing pairs of {111} diffraction spots, the maximum of one pair is about 8°–15° off the rolling direction and of the other is about 55°–67° off the rolling direction. c. STEM-HAADF image within the shear band showing stack faults and twinning in one Ag lamella surrounded by Cu lamellae. The < 111 > interplanar spacing of the Ag lamella (0.25 nm) is 1.12 times that of the Cu lamellae (0.21 nm).

Because the reduction-in-thickness for the sheets used in the current study varied less than 1% from those used in earlier studies, we assumed that the texture in our 0.67 mm-thick sheets was also < 111 > in the longitudinal direction. This assumption was confirmed by our TEM work (Fig. 4). If [111] (i.e., one of the < 111 > directions) is assumed to be parallel to the tensile axis in longitudinal samples, then [11-1] (another of the < 111 > directions) would form a 70.5° angle with [111], the tensile axis. The slip bands in our samples were oriented in the 60° direction, i.e., about 10° off the (11-1) planes and 15° off the maximum shear stress plane (45° off the tension axis). We assumed that the slight increase in shear stress associated with necking was amplified in our longitudinal samples by the formation of small consistent angles between the (11-1) planes and the maximum shear stress plane. Subsequently, the presence of more numerous slip systems on {111} planes resulted in even shorter necking regions. In transversal tensile samples, by contrast, the slip systems on {111} planes had large, inconsistent angles with the maximum shear stress plane. These angles were probably the reason why the slip bands in transversal samples were inclined more closely to the maximum shear stress plane, resulting in longer and less localized regions in which necking could occur.

Rolling direction-dependent shear bands analyses

Proceeding on the assumption that the difference in strain-hardening between longitudinal and transversal samples was caused by microstructure differences, we examined our sheets using various microscopy methods. On longitudinal x-sections, we observed many continuous shear bands (Fig. 4a). They penetrated multiple lamellae. The average spacing between these bands was above 8 µm, and the density was about 0.02 μm^{-1}. Their length varied from 80 to ~ 800 µm. The angle between these shear bands and the sheet rolling direction was in a range of 30°–40°, which is very typical in cold-rolled materials[33]. The angle between the shear bands and (11-1) plane in microscale was between 8° and 15° (Fig. 4b). In other words, the shear bands appeared mostly on irrational crystallographic planes because the orientation of the shear bands did not match any single low-indexed crystallographic plane. Such shear bands have been referred to as non-crystallographic deformation zones [34]. These bands, which are the result of plastic instability, often carry the highly localized shears that form during rolling deformation. The behavior of these bands is similar to the 'necking' that sometimes occurs in tensile tests [34, 35].

Therefore, the presence of these large number of existing shear bands may be responsible for the ~ 10 ° deflection of the slip bands from the (11-1) plane. We speculated that, during tension deformation, long shear bands most likely provided the path for dislocation gliding. We observed that, within these shear bands, the lamellar thickness values of Cu and Ag were below 6 nm and 2 nm, respectively (Fig. 4b). The lattice parameter difference between Cu and Ag in our materials was smaller than that between bulk Cu and Ag samples, indicating that the lattice had become distorted to reduce internal stress in nanoscale lamellae. Even so, the existing lattice misfit near interfaces resulted in compression internal stress in Ag and tension internal stress in Cu [36]. The magnitude of internal stress varied according to measurement orientation. It was difficult for dislocations to accumulate in samples with distorted crystal lattices because of the presence of refined lamellae.

In Ag, we observed both stacking faults and twins (Fig. 4c). These defects may strengthen the composite in certain cases, but once the stress is applied, partial dislocations may propagate at triple joints located on interfaces. The interfaces between Cu and Ag took the familiar zigzag form seen in heavily deformed samples, but they were more distinct than we expected, indicating that the shear caused by partial dislocations had not brought about the significant dissolution of Ag in Cu. One of the reasons behind the formation of zigzag interfaces is to lower interfacial energy between Ag and Cu so that most of the interfaces remain on the {111} planes. The presence of low interface energy prohibits the dissolution of Ag in Cu.

In longitudinal samples, the presence of shear band angles, twins, refined lamellae, and rough interface structure may have been the reason for the prevalence of softening. By contrast, in transversal samples (where shear bands were practically nonexistent with respect to loading), the presence of straight lamellae probably allowed for more accumulation of dislocations and consequently greater hardening.

Conclusions

1. In this work, we studied strain-hardening behavior in high-strength Cu–Ag sheets by comparing *overall* stress–strain curves with *local* stress–strain curves. Engineering stress–strain curves showed both overall and local softening in both longitudinal and transversal samples. These curves showed no hardening at all in any of the samples. True stress–strain curves also showed overall softening, but no hardening, in both longitudinal and transversal samples. In regions with highly strained slip bands, however, a different strain-hardening trend was discovered. True stress–strain curves showed pronounced local strain-hardening in transversal tensile samples, but only strain-softening in longitudinal ones. Such anisotropy of plasticity occurred only in very local necking regions (~ 1.4 mm in width).
2. We observed many shear bands in longitudinal cross-section, but not in transversal. Microscale examination revealed shear bands running 8°-15° off the {111} orientation. In longitudinal cross-section samples, we observed stacking faults and twins within the shear bands, indicating severe plastic deformation resulting mainly from the propagation of partial dislocations.
3. The existence of complex interrelationships among shear band orientations, crystallographic orientations, and interface orientations meant that measurable strain-hardening and strain-softening were both dependent on the rolling direction. Strain-softening in longitudinal tensile samples was the result of the favorable angle within shear bands between the maximum shear stress direction and the existing slip system on {111}. Conversely, strain-hardening in transversal tensile samples was the result of the absence of such angles.

We speculated that strain-hardening in longitudinal samples could be increased either by producing shear bands in other orientations or by reducing rolling strain enough to produce fewer shear bands.

Acknowledgements

The work was undertaken in the National High Magnetic Field Laboratory, which is supported by NSF DMR-1644779 and the State of Florida. We thank Dr. Tyler for the paper editing.

Declarations

Conflict of interest The authors declare that they have no known competing financial interests or personal relationships that could have appeared to influence the work reported in this paper.

Data and code availability The data that support the findings of this study are available on request from the corresponding author.

Ethical approval Not Applicable.

Supplementary Information: The online version contains supplementary material available at https://doi.org/10.1007/s10853-023-08519-y.

References

[1] Deng L, Wang B, Han K et al (2019) Response of microstructure to annealing in in situ Cu–Nb microcomposite. J Mater Sci 54:840–850. https://doi.org/10.1007/s10853-018-2865-4

[2] Han K, Embury JD, Petrovic JJ, Weatherly GC (1998) Microstructural aspects of Cu–Ag produced by the Taylor wire method. Acta Mater 46:4691–4699. https://doi.org/10.1016/S1359-6454(98)00135-9

[3] Han K, Embury JD, Sims JR et al (1999) The fabrication, properties and microstructure of Cu–Ag and Cu–Nb composite conductors. Mater Sci Eng, A 267:99–114. https://doi.org/10.1016/S0921-5093(99)00025-8

[4] Niu R, Toplosky V, Han K (2022) Cryogenic temperature properties and secondary phase characterization of CuCrZr composites. IEEE Trans Appl Supercond 32:1–5. https://doi.org/10.1109/TASC.2022.3152992

[5] Sakai Y, Inoue K, Maeda H (1994) High-strength and high-conductivity Cu–Ag alloy sheets: new promising conductor for high-fieId Bitter coils. IEEE Trans Magn 30:2114–2117. https://doi.org/10.1109/20.305687

[6] Sakai Y, Inoue K, Maeda H (1995) New high-strength, high-conductivity Cu–Ag alloy sheets. Acta Metall Mater 43:1517–1522. https://doi.org/10.1016/0956-7151(94)00376-S

[7] Spitzig WA, Downing HL, Laabs FC, Gibson ED, Verhoeven JD (1993) Strength and electrical conductivity of a deformation-processed Cu-5 Pct Nb composite. Metall Trans A 24:7–14. https://doi.org/10.1007/BF02669596

[8] Spitzig WA, Krotz PD (1988) Comparison of the strengths and microstructures of Cu-20% Ta and Cu-20% Nb in situ composites. Acta Metall 36:1709–1715. https://doi.org/10.1016/0001-6160(88)90238-6

[9] Thilly L, Véron M, Ludwig O, Lecouturier F, Peyrade JP, Askénazy S (2002) High-strength materials: in-situ investigations of dislocation behaviour in Cu-Nb multifilamentary nanostructured composites. Philos Mag A 82:925–942. https://doi.org/10.1080/01418610208240010

[10] Verhoeven JD, Spitzig WA, Jones LL et al (1990) Development of deformation processed copper-refractory metal composite alloys. J Mater Eng 12:127–139. https://doi.org/10.1007/BF02834066

[11] Verhoeven JD, Spitzig WA, Schmidt FA, Krotz PD, Gibson ED (1989) Processing to optimize the strength of heavily drawn Cu-Nb alloys. J Mater Sci 24:1015–1020. https://doi.org/10.1007/BF01148792

[12] An B, Xin Y, Niu R et al (2022) Stacking fault formation and Ag precipitation in Cu–Ag-Sc alloys. Mater Charact 189:111965. https://doi.org/10.1016/j.matchar.2022.111965

[13] An B, Xin Y, Niu R, Xiang Z, Wang E, Han K (2022) Nucleation and growth of discontinuous precipitates in Cu–Ag alloys. Mater Res Express 9:026530. https://doi.org/10.1088/2053-1591/ac5775

[14] Deng L-P, Wang B-S, Xiang H-L, Yang X-F, Niu R-M, Han K (2016) Effect of annealing on the microstructure and properties of in-situ cu–nb microcomposite wires. Acta Metall Sin (Eng Lett) 29:668–673. https://doi.org/10.1007/s40195-016-0432-z

[15] Han K, Goddard R, Niu R et al (2016) Bending behavior of high-strength conductor. IEEE Trans Appl Supercond 26:1–4. https://doi.org/10.1109/TASC.2016.2517412

[16] Han K, Niu R, Lu J, Toplosky V (2016) High strength conductors and structural materials for high field magnets. MRS Adv 1:1233–1239. https://doi.org/10.1557/adv.2016.264

[17] Zhao C, Niu R, Xin Y et al (2021) Improvement of properties in Cu–Ag composites by doping induced microstructural refinement. Mater Sci Eng A 799:140091. https://doi.org/10.1016/j.msea.2020.140091

[18] Aasi A, Aghaei SM, Panchapakesan B Noble metal (Pt or Pd)-decorated atomically thin MoS2 as a promising material for sensing colorectal cancer biomarkers through exhaled breath. Int J Comput Mater Sci Eng 0: 2350014. https://doi.org/10.1142/s2047684123500148

[19] Sakai Y, Schneider-Muntau HJ (1997) Ultra-high strength, high conductivity Cu–Ag alloy wires. Acta Mater 45:1017–1023. https://doi.org/10.1016/S1359-6454(96)00248-0

[20] Davy CA, Han K, Kalu PN, Bole ST (2008) Examinations of Cu–Ag composite conductors in sheet forms. IEEE Trans Appl Supercond 18:560–563. https://doi.org/10.1109/TASC.2008.922510

[21] Han K, Vasquez AA, Xin Y, Kalu PN (2003) Microstructure and tensile properties of nanostructured Cu-25wt%Ag. Acta

Mater 51:767–780. https://doi.org/10.1016/S1359-6454(02)00468-8

[22] Niu R, Han K, Xiang Z, Qiao L, Siegrist TM (2020) Ultra-high local plasticity in high-strength nanocomposites. J Mater Sci 55:15167–15182. https://doi.org/10.1007/s10853-020-05076-6

[23] Shen TD, Zhang X, Han K et al (2007) Structure and properties of bulk nanostructured alloys synthesized by flux-melting. J Mater Sci 42:1638–1648. https://doi.org/10.1007/s10853-006-1096-2

[24] Niu R, Han K (2013) Cross-section metal sample preparations for transmission electron microscopy by electro-deposition and electropolishing. Microsc Res Tech 76:476–480. https://doi.org/10.1002/jemt.22189

[25] Kamaya M (2009) A procedure for estimating Young's modulus of textured polycrystalline materials. Int J Solids Struct 46:2642–2649. https://doi.org/10.1016/j.ijsolstr.2009.02.013

[26] Mullen RL, Ballarini R, Yin Y, Heuer AH (1997) Monte Carlo simulation of effective elastic constants of polycrystalline thin films. Acta Mater 45:2247–2255. https://doi.org/10.1016/S1359-6454(96)00366-7

[27] Broberg KB (1999). In: Broberg KB (ed) Cracks and fracture. Academic Press, San Diego

[28] Banabic D (2000). In: Banabic D, Bunge HJ, Pöhlandt K, Tekkaya AE, Banabic D (eds) Formability of metallic materials: plastic anisotropy, formability testing, forming limits. Springer, Berlin

[29] Glavas V (2017), Karlsruher Institut für Technologie (KIT)

[30] Bao C, Francois M, Le Joncour L (2016) A closer look at the diffuse and localised necking of a metallic thin sheet: evolution of the two bands pattern. Strain 52:244–260. https://doi.org/10.1111/str.12184

[31] Cazacu O, Rodríguez-Martínez JA (2019) Effects of plastic anisotropy on localization in orthotropic materials: New explicit expressions for the orientation of localization bands in flat specimens subjected to uniaxial tension. J Mech Phys Solids 126:272–284. https://doi.org/10.1016/j.jmps.2019.03.002

[32] Hill R (2001) On the mechanics of localized necking in anisotropic sheet metals. J Mech Phys Solids 49:2055–2070. https://doi.org/10.1016/S0022-5096(01)00031-X

[33] Raabe D (2014) in Laughlin DE, Hono K (eds)Physical Metallurgy (Fifth Edition)Elsevier, Oxford

[34] Humphreys FJ, Hatherly M (eds) (2004) 2nd edn. Elsevier, Oxford

[35] Jia N, Roters F, Eisenlohr P, Kords C, Raabe D (2012) Non-crystallographic shear banding in crystal plasticity FEM simulations: Example of texture evolution in α-brass. Acta Mater 60:1099–1115. https://doi.org/10.1016/j.actamat.2011.10.047

[36] Han ¶ K, Lawson AC, Wood JT, Embury JD, Von Dreele RB, Richardson JW (2004) Internal stresses in cold-deformed Cu–Ag and Cu–Nb wires. Philos Mag 84:2579–2593. https://doi.org/10.1080/14786430410001689981